

Cite this: *Catal. Sci. Technol.*, 2014, 4, 3474

Open Access Article. Published on 03 June 2014. Downloaded on 28.01.2026 20:35:41.
This article is licensed under a Creative Commons Attribution 3.0 Unported Licence.

Mechanism of CO₂ hydrogenation to formates by homogeneous Ru-PNP pincer catalyst: from a theoretical description to performance optimization†

Georgy A. Filonenko,^{ab} Emiel J. M. Hensen^{ab} and Evgeny A. Pidko^{*ab}

The reaction mechanism of CO₂ hydrogenation by pyridine-based Ru-PNP catalyst in the presence of DBU base promoter was studied by means of density functional theory calculations. Three alternative reaction channels promoted by the complexes potentially present under the reaction conditions, namely the dearomatized complex **2** and the products of cooperative CO₂ (**3**) and H₂ (**4**) addition, were analysed. It is shown that the bis-hydrido Ru-PNP complex **4** provides the unique lowest-energy reaction path involving a direct effectively barrierless hydrogenolysis of the polarized complex **5***. The reaction rate in this case is controlled by the CO₂ activation by Ru-H that proceeds with a very low barrier of *ca.* 20 kJ mol⁻¹. The catalytic reaction can be hampered by the formation of a stable formato-complex **5**. In this case, the rate is controlled by the H₂ insertion into the Ru-OCHO coordination bond, for which a barrier of 65 kJ mol⁻¹ is predicted. The DFT calculations suggest that the preference for the particular route can be controlled by varying the partial pressure of H₂ in the reaction mixture. Under H₂-rich conditions, the former more facile catalytic path should be preferred. Dedicated kinetic experiments verify these theoretical predictions. The apparent activation energies measured at different H₂/CO₂ molar ratios are in a perfect agreement with the calculated values. Ru-PNP is a highly active CO₂ hydrogenation catalyst allowing reaching turnover frequencies in the order of 10⁶ h⁻¹ at elevated temperatures. Moreover, a minor temperature dependency of the reaction rate attainable in excess H₂ points to the possibility of efficient CO₂ hydrogenation at near-ambient temperatures.

Received 2nd May 2014,
Accepted 31st May 2014

DOI: 10.1039/c4cy00568f

www.rsc.org/catalysis

Introduction

Utilization of CO₂ as a renewable C1 building block in chemical synthesis is recognized as a key strategy for developing more sustainable chemical technologies.^{1–4} Considerable attention has been devoted to CO₂ coupling reactions for the production of cyclic carbonates or carboxylic acid derivatives.^{5–10} Alternatively, CO₂ can be hydrogenated to C1 chemicals, such as formic acid (FA)^{11,12} and, more challenging, methanol.^{13–15} In addition to being important chemical intermediates, these compounds can be utilized as hydrogen storage agents as long as the reverse dehydrogenation reaction can be made to produce only carbon dioxide as the byproduct.^{16–20} Fully reversible

processes for H₂ storage/release have so far only been demonstrated for the CO₂/FA pair.^{18–24}

The hydrogenation of carbon dioxide to formates has been the subject of many experimental and theoretical studies. The main focus has been on homogeneous catalysts, some of them with very high activity for the formation of formates and also their decomposition.^{25–29} Most of the homogeneous systems make use of noble metals,^{30,31} although a substantial progress has recently been made using first-row transition metal, namely, Fe^{32,33} and Co³⁴ complexes. Despite the apparent simplicity of the overall reaction, the mechanism of the catalytic CO₂ hydrogenation by homogeneous catalysts is still under debate. One of the first examples of an active catalyst for CO₂ hydrogenation under supercritical conditions, [Ru(H)₂(PMe₃)₃]³⁵ has been studied computationally by Sakaki and co-workers.^{36,37} The authors identified CO₂ insertion into the Ru-H bond as the rate determining step (RDS) under water free conditions, whilst the coordination of H₂ to Ru-formate species was shown to determine the reaction rate in the presence of water. A subsequent detailed investigation by Urakawa *et al.* revealed that CO₂ insertion is a facile

^a Inorganic Materials Chemistry, Department of Chemical Engineering, Eindhoven University of Technology, P.O. Box 513, 5600 MB Eindhoven, The Netherlands.

E-mail: e.a.pidko@tue.nl

^b Institute for Complex Molecular Systems, Eindhoven University of Technology, P.O. Box 513, 5600 MB Eindhoven, The Netherlands

† Electronic supplementary information (ESI) available: Reaction free energy diagrams for catalysis by **4** in DMF, results of small-scale CO₂ hydrogenation experiments with **1**. See DOI: 10.1039/c4cy00568f

process, whereas the H_2 insertion in the Ru-formate complex represents the rate determining step for $[\text{Ru}(\text{dmpe})_2\text{H}_2]\text{-catalysed CO}_2$ hydrogenation.³⁸ These findings were used to rationalize the increased activity at elevated H_2 partial pressure, which represented a major inconsistency with the earlier proposal on the RDS nature of the CO_2 insertion step.

Substantial progress in the catalytic CO_2 hydrogenation was made when Ir-PNP pincer complexes were introduced as catalysts by Nozaki³⁹ and co-workers in 2009. The presence of a non-innocent PNP pincer ligand, which can be directly involved in chemical transformations in the course of the catalytic reaction,^{40–42} increases the complexity with respect to the mechanistic analysis. In the presence of a base, the PNP ligands can be deprotonated resulting in formation of a basic cooperative site on the side-arm of the dearomatized PNP* ligand that can participate in substrate activation^{40,41} (see Scheme 1 for a related reaction for Ru-PNP complex, 1 → 2). As a result, two alternative pathways were proposed for the hydrogenation of CO_2 over Ir-PNP,⁴³ the first of which involves the deprotonative ligand dearomatization as the key reaction step. The alternative mechanism involves the OH^- -assisted hydrogen cleavage in the H_2 σ -complex, which regenerates the initial state of the catalyst, as the RDS. The latter mechanism was supported in a theoretical study by Yang⁴⁴ and Ahlquist⁴⁵ who found that the direct base-assisted H_2 cleavage was more favourable than pathways involving the ligand participation. A similar conclusion was drawn for iron- and cobalt-based PNP catalysts.

Recently, the application of ruthenium pincer catalysts in CO_2 hydrogenation has been described.^{46,47} The corresponding ruthenium pincer complexes bearing pyridine-based PNN and PNP ligands are known to reversibly bind CO_2 ^{48,49} via a metal-ligand cooperative mechanism (2 → 3, Scheme 1). The resulting products of [1,3]- CO_2 addition can contribute to the overall performance of these catalysts in the hydrogenation reaction. Huff and Sanford⁴⁶ reported that Ru-PNN pincer⁵⁰ catalyst can be used for hydrogenation of CO_2 to formates with a rate (turnover frequency, TOF) of 2200 h^{-1} . A mechanism involving the dearomatization of the PNN ligand has been proposed. This proposal was confirmed in reactivity studies, employing $\text{KO}^\text{t}\text{Bu}$ to liberate HCOO^- at the end of

the catalytic cycle. However, the possibility of ligand deprotonation with catalytically superior K_2CO_3 base has not been confirmed yet.

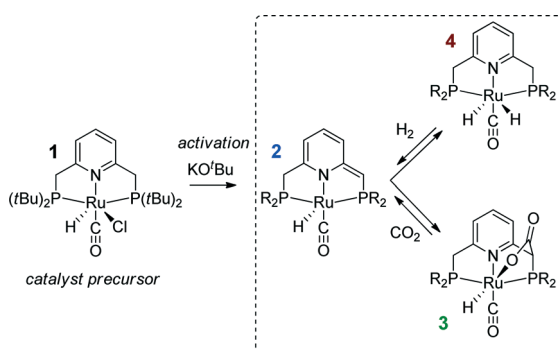
Previously, we have demonstrated that a related Ru-PNP catalyst 1 (ref. 50) (Scheme 1) shows remarkable catalytic performance in reversible CO_2 hydrogenation.^{22,47} In a previous communication,⁴⁷ we investigated the mechanism of the catalytic reaction by a combination of kinetic experiments and *in situ* NMR experiments supported by DFT calculations. The results pointed to the inhibiting effect of the CO_2 adduct 3 on catalytic performance. In agreement with previous reports,^{38,43,44} bis-hydrido Ru species were postulated as the active state. It was argued that the dearomatized Ru-PNP* complex 2 did not contribute to the catalytic reaction. Nevertheless, the contribution of multiple reaction paths involving different species (Scheme 2) cannot be omitted and careful mechanistic analysis is required.

Herein, we present a systematic DFT study of the CO_2 hydrogenation to formates by Ru-PNP complexes that can be formed under reaction conditions. The catalytic cycles over the bis-hydrido complex 4, the dearomatized species 2 and the CO_2 -adduct 3 were considered (Scheme 2). This work is a continuation of our previous mechanistic study.⁴⁷ The main focus will be on the analysis of the reaction networks underlying the catalytic process to identify the catalytic role of different intermediates present in the reaction mixture. The theoretical insights are validated by dedicated experiments.

Computational and experimental details

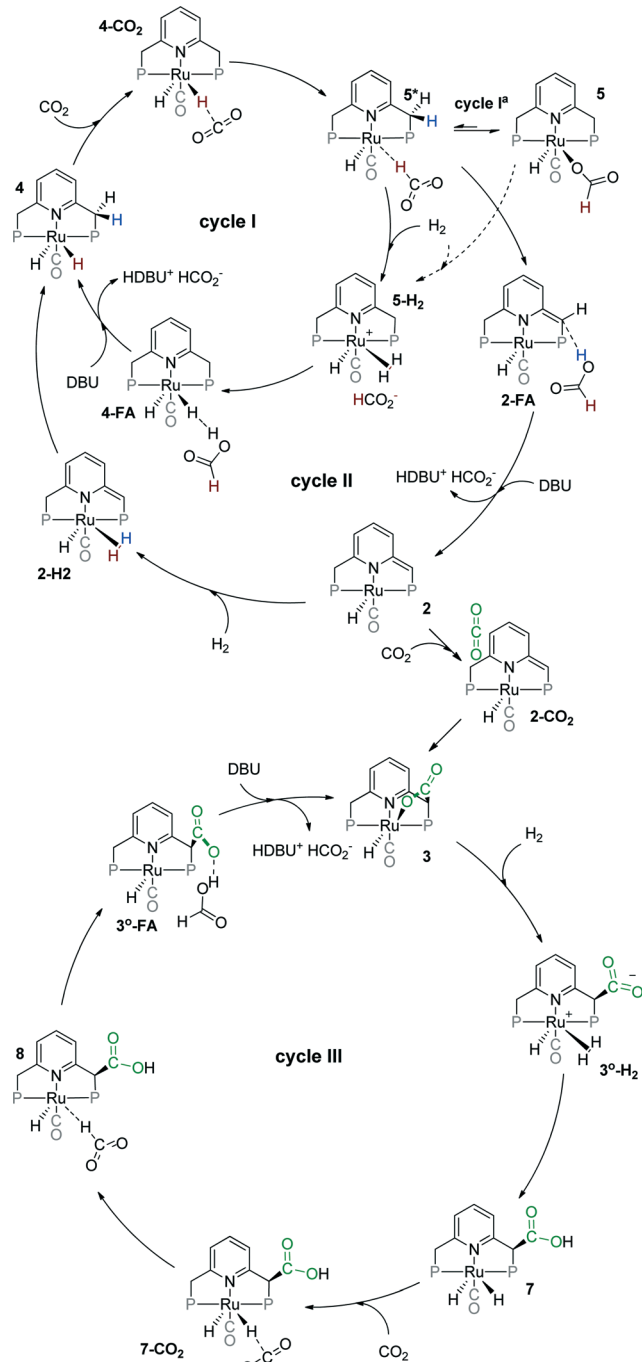
Density functional theory calculations

Similar to our previous work,⁴⁷ density functional theory (DFT) calculations were performed with the PBE0 (also denoted as PBE1PBE and PBEh)⁵¹ hybrid exchange-correlation functional using Gaussian 09, revision D.01 program.⁵² The high accuracy of this method has been demonstrated by previous benchmark studies on a wide set of different chemical systems^{53,54} and by our own accuracy tests employing different DFT methods for modelling CO_2 hydrogenation to formic acid.⁴⁷ The full electron 6-311G(d,p) basis set^{55,56} was used for all atoms except ruthenium, for which the LanL2DZ basis set^{57,58} was employed. The polarisable continuum model (PCM) with standard parameters for THF and DMF solvents, as implemented in the Gaussian 09 rev. D.01 program package, was used during the geometry optimization and frequency analysis to account for bulk solvent effects. Because the differences in reaction free energies computed with PCM model of THF and DMF solvents do not exceed 5 kJ mol^{-1} (see ESI†), only the results obtained for the THF solvent are discussed here. The accuracy of this computational method was tested by calculating energetics of selected elementary reaction steps (2 + H_2 → 4 (ref. 47) and 4 + CO_2 → 5*, Scheme 1) using a larger triple-zeta + polarization quality basis set combination employing Def2-TZVPP⁵⁹ basis set for the Ru centre and 6-311+G(d,p) for the light atoms. The resulting reaction and activation energies agreed



Scheme 1 Activation of a Ru-PNP precursor 1 by deprotonation with a strong base and the subsequent metal-ligand cooperative activation of CO_2 and H_2 .





Scheme 2 Possible catalytic cycles for CO_2 hydrogenation to formates by Ru-PNP pincer complexes (^tBu substituents of the ligand are omitted for clarity).

within 5 kJ mol^{-1} with those obtained using the standard methodology (see ESI[†] and ref. 47). Note that the expansion of the basis set with diffuse functions has a negligible effect on the computed energetics, while it resulted in a much slower SCF convergence (when PCM model was used to account for solvent effects).

The nature of the stationary points was evaluated from the analytically computed harmonic modes. No imaginary

frequencies were found for the optimized structures, confirming that these correspond to local minima on the potential energy surface. All transition states exhibited a single imaginary frequency, corresponding to the eigenvector along the reaction path. The assignment of the transition state structure to a particular reaction path was tested by perturbing the structure along the reaction path eigenvector in the directions of the product and the reagent followed by geometry optimization. For catalytic cycles I, II and III starting from the activated species 3°-H_2 IRC calculations were performed to additionally confirm the assignment of the transition states. The reaction (ΔE) and activation energies (E^\ddagger) reported in the manuscript were corrected for zero point (E_{ZPE}) energy contribution computed using the results of the normal-mode analysis. Free energy values (ΔG°) were computed using the results of the normal-mode analysis within the ideal gas approximation at a pressure of 1 atm and temperatures of 298 K.

Catalytic CO_2 hydrogenation

All manipulations unless otherwise stated were performed using Schlenk techniques. Argon was dried with a Sicapent column. Air sensitive compounds were stored in a MBraun glovebox under an atmosphere of dry nitrogen or argon. Solvents were dispensed from MBraun solvent purification system. 1,8-Diazabicyclo[5.4.0]undec-7-ene (DBU) was purchased from Fluorochem and vacuum distilled from calcium hydride. Catalyst 1 was prepared according to original literature procedure.⁶⁰

Small scale CO_2 hydrogenation experiments were performed in A96 parallel reactor at 70 °C under 40 bar of equimolar $\text{H}_2\text{-CO}_2$ mixture. In a typical experiment 3 mL THF or DMF, and appropriate amount of base DBU (3.3 mmol) or $\text{KO}^\ddagger\text{Bu}$ (0.33 mmol) were mixed with 0.1 μmol of catalyst. The reaction was quenched after 2 hours by addition of water-ethanol mixture and immediately analyzed. Concentrations of formic acid were analyzed using Shimatzu HPLC setup with 25 mM phosphate buffer of pH = 2 as mobile phase using Prevail Organic Acid column. GC measurements, where appropriate, were performed using Shimatzu GC-17A instrument.

Kinetic measurements were carried out in Top Industrie 100 mL stainless steel autoclave. The vessel was evacuated overnight at 150 °C, purged several times with Ar, and the reaction medium was introduced by cannulae transfer. The autoclave was flushed with $\text{H}_2\text{-CO}_2$ mixture or hydrogen, preheated to reaction temperature and filled with $\text{H}_2\text{-CO}_2$ mixture up to operating pressure of 40 bar. The catalyst was then introduced *via* a dosage device and the reaction started. Constant pressure was maintained by a compensation device fitted with Bronkhorst EL-FLOW MFC unit and digital pressure meter with equimolar $\text{H}_2\text{-CO}_2$ mixture. Samples were withdrawn *via* dip-tube installation (dead volume 4 μL , sampling volume 110 μL), diluted to 1 mL and immediately analysed by HPLC and GC-FID. In a typical experiment 30 mL solvent, 5 mL DBU (33.4 mmol), 1 mL toluene or THF (used



as an internal standard) and appropriate amount of catalysts dispensed from the stock solution were used. The kinetic traces represent single run results.

Results and discussion

Catalyst activation

Hydrogenation activity of Ru-PNP pincer is usually initiated by reacting a catalyst precursor **1** with a strong base to form a dearomatized Ru-PNP* species **2** (Scheme 1). Both substrates of the catalytic CO₂ hydrogenation reaction, namely, CO₂ and H₂ can then undergo a metal-ligand cooperative addition to **2** resulting in rearomatized Ru-PNP complexes **3**⁴⁹ and **4**,^{50,61} respectively. Fig. 1 shows the optimized structures of the involved reaction intermediates and transition states together with the computed energetics of the elementary reaction steps.⁴⁷ The reaction starts with the formation of molecular complexes of **2** with the substrate molecules. Despite very similar thermodynamics of complexation with CO₂ and H₂, the nature of the formed species is quite different. Whereas no specific interaction between CO₂ and Ru-PNP* is observed in 2-CO₂, 2-H₂ represents a classical example of a σ-H₂ complex^{62–66} featuring a highly symmetric η^2 -coordination of dihydrogen with short Ru-H distances and a considerably elongated H-H bond ($r(\text{H-H}) = 0.821 \text{ \AA}$ vs. 0.747 Å for the free molecule).

The cooperative [1,3]-addition of CO₂ (2-CO₂ \rightarrow TS₂₋₃ \rightarrow 3) is exothermic by -51 kJ mol^{-1} and proceeds with a low activation barrier of 34 kJ mol^{-1} . When corrected for entropic effects, the reaction and activation Gibbs free energies are, respectively, equal to -31 and 50 kJ mol^{-1} . This evidences a pronounced entropy loss due to the decrease in the degrees of freedom upon the chemical binding of the non-specifically coordinated CO₂. The TS₂₋₃ is an early transition state that features a distorted CO₂ molecule that forms rather elongated bonds with the basic C1 site of the ligand ($r(\text{C1-C2}) = 2.543 \text{ \AA}$) and the Ru center ($r(\text{Ru-O1}) = 2.537 \text{ \AA}$). The structural properties of TS₂₋₃ suggest that the dominant destabilizing contribution to the activation energy in this case is associated with the bending of the linear CO₂ molecule necessary for the attack by the basic C1 centre at the PNP* pincer arm. The promoting effect of the concomitant coordination to Ru is the polarization of the CO₂ molecule and stabilization of the negative charge at the O1 atom (Mulliken atomic charge in TS₂₋₃ is -0.280 e^-) in the course of the [1,3]-addition reaction towards **3**. The optimized structure of **3** agrees well with the single-crystal X-ray diffraction data reported by Milstein and co-workers.⁴⁹ The accuracy of the current computational method is supported by a good match between the calculated E^\ddagger and G^\ddagger (85 and 81 kJ mol^{-1} , respectively) and the experimental values (94 and 83 kJ mol^{-1})⁴⁹ determined for the reverse $3 \rightarrow 2 + \text{CO}_2$ transformation.

Dissociation of H₂ over **2** gives a bis-hydrido Ru-PNP complex **4** (2-H₂ \rightarrow TS₂₋₄ \rightarrow **4**, Fig. 1) and proceeds with an activation barrier ($E_{ZPE}^\ddagger = 75 \text{ kJ mol}^{-1}$) substantially higher than that computed for the reaction with CO₂. Because H₂ is effectively immobilized within the σ-complex 2-H₂, the entropic contribution to the reaction and activation energy in this case is negligible. As a result the overall reaction $2 + \text{H}_2 \rightarrow 4$ ($\Delta G^\circ = -40 \text{ kJ mol}^{-1}$) is more thermodynamically favourable than the reaction with CO₂ ($2 + \text{CO}_2 \rightarrow 3$, $\Delta G^\circ = -8 \text{ kJ mol}^{-1}$). In the TS₂₋₄, the polarized H₂ molecule undergoes a heterolytic cleavage over a Ru···C1 acid-base pair. The calculated Mulliken charges on the H1 and H2 atoms in TS₂₋₄ are -0.056 and 0.187 e^- , respectively. The high activation barrier in this case is most likely due to the relatively large distance between the acid and the base sites in the dearomatized Ru-PNP* (**2**: $r(\text{C1} \cdots \text{Ru}) = 3.191 \text{ \AA}$) that hampers the efficient stabilization of both the H[−] and H⁺ species formed in the transition state.

An insight into the origin of the different coordination behaviour and reactivity of **2** towards CO₂ and H₂ can be obtained from the frontier orbital analysis (Fig. 3). An unoccupied d_{2z} orbital on Ru and an occupied formally p_z orbital on basic C1 contribute mostly to the LUMO and HOMO of **2**. HOMO-1 is dominated by an occupied Ru d_{yz} orbital. These molecular orbitals (MOs) cannot form a positive overlap with the π* LUMO and n HOMO orbitals of linear non-perturbed CO₂. Their linear combination leads to a non-bonding interaction. This explains the non-specific coordination of carbon dioxide in 2-CO₂. The change of hybridization of the C atom in CO₂ upon bending (CO₂^{*}) make a positive orbital overlap

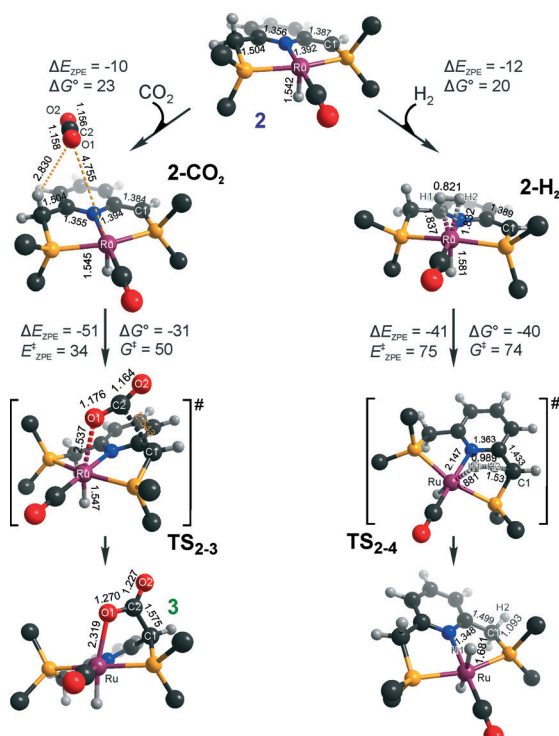


Fig. 1 Optimized structures of reaction intermediates and transition states involved in the metal-ligand cooperative activation of H₂ and CO₂ by **2** (in the graphical representation ¹Bu substituents at the phosphine moieties are simplified for clarity). ZPE-corrected reaction (ΔE_{ZPE}) and activation energies (E_{ZPE}^\ddagger), reaction and activation Gibbs free energies (ΔG° and G^\ddagger) are given in kJ mol^{-1} (for individual elementary steps).⁴⁷



between LUMO of CO_2^* and HOMO of 2 possible. The relatively small energy gap between these orbitals enhances the acid–base interaction resulting in a very low barrier of the [1,3]-addition of CO_2 to 2.

HOMO σ and LUMO σ^* orbitals of H_2 can be involved in donation and back-donation interactions with LUMO and HOMO – 1 orbitals of 2, respectively, in 2– H_2 σ -complex. However, because of the large energy difference between the interacting orbitals, binding within the molecular complex is weak (Fig. 1). The specific coordination of H_2 to 2 promotes the formation of 4. In support of the above proposition, the high energy barrier for H_2 dissociation is due to the distant location of the base site. Indeed, the complexation with H_2 does not change the properties of the HOMO.

These results suggest that the preference towards the formation of complexes 3 and 4 during the catalytic CO_2 hydrogenation can be altered by varying the reaction conditions. Indeed, whereas the reaction of 2 with H_2 to the bis-hydrido complex 4 is more thermodynamically favourable, the alternative path towards the CO_2 adduct 3 proceeds with a much lower activation barrier. This implies that by increasing partial pressure of H_2 in the reaction mixture, the formation of 4 can be promoted. However, in the presence of excess base necessary to promote catalytic CO_2 hydrogenation, one cannot exclude the transient formation of the dearomatized species 2, which can also contribute to the catalytic activity of the Ru-PNP catalyst. To understand the behaviour of this system, analysis of reaction paths over these three alternative potentially active species is necessary.

CO_2 hydrogenation over 4

The calculated reaction energy diagram for the catalytic cycle I (Scheme 2) of CO_2 hydrogenation by bis-hydrido Ru-PNP complex 4⁴⁷ is shown in Fig. 3. The starting point of the reaction is an energy-neutral binding of CO_2 to 4 resulting in 4– CO_2 . Weak intermolecular contacts between the O atoms of CO_2 and acidic CH_2 protons of the PNP pincer arms in 4– CO_2 ($r(\text{O}\cdots\text{H}) = 2.584 \text{ \AA}$) direct the CO_2 coordination towards the Ru–H moiety. This allows a facile attack of CO_2 by Ru-bound hydride (Mulliken charge on the Ru-bound H atom is -0.152 e^-) resulting in a formate anion ($4\text{--CO}_2 \rightarrow \text{TS}_{4-5} \rightarrow 5^*$). The reaction is exothermic by -13 kJ mol^{-1} and shows a very low activation barrier of 23 kJ mol^{-1} . Similar to [1,3]- CO_2 addition to 2, the reaction is triggered by the increased acidity of the sp^2 -like C atom in bent CO_2 moiety formed in TS_{4-5} that ensures an efficient overlap between the s orbital of the H^- ligand being one of the main contributors of HOMO (4) and LUMO of CO_2^* (Fig. 2). Note that HOMO in complex 4 lies 1 eV lower than that in 2 indicating a lower nucleophilicity of the H^- ligand compared to the basic C1 centre in complexes 4 and 2, respectively. This is in line with the much higher exothermicity of the cooperative CO_2 activation by 2.

At the next step Ru–H-coordinated HCOO^- anion is replaced by H_2 yielding a cationic σ - H_2 Ru-PNP complex

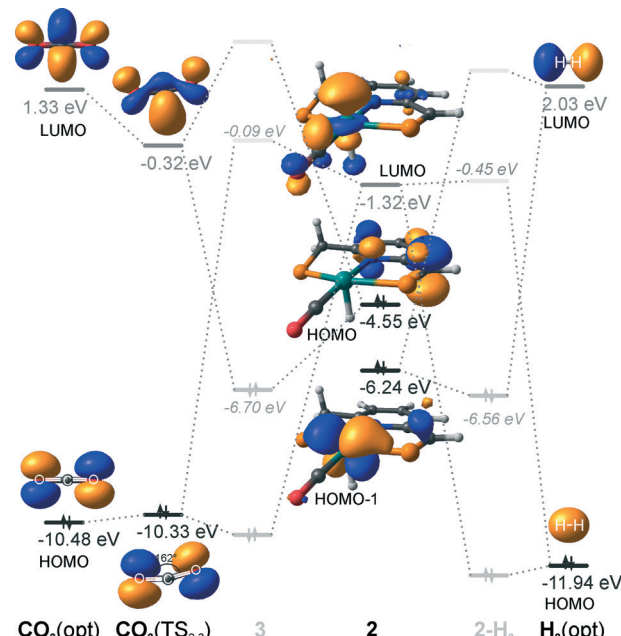


Fig. 2 Frontier orbitals of the dearomatized complex 2 optimized H_2 and CO_2 molecules ($\text{H}_2(\text{opt})$ and $\text{CO}_2(\text{opt})$) as well as those of the bent CO_2 moiety from the TS_{2-3} structure ($\text{CO}_2(\text{TS}_{2-3})$). ^3Bu at the phosphine moieties in 2 are omitted for clarity, while the respective MO contributions are visualized. Dotted lines depict possible orbital interactions following simplified symmetry considerations and solid grey lines represent the qualitative energetics of the resulting MOs in complexes 3 and 2– H_2 with the energy values indicated for the orbitals, for which the contribution of the interacting molecular fragments could be unambiguously defined.

charge-compensated by HCOO^- hydrogen bonded with the CH_2 moieties of the ligand ($5^* + \text{H}_2 \rightarrow 5\text{--H}_2$). Subsequent heterolytic dissociation of H_2 over an acid–base pair composed of the Ru centre and the adjacent formate anion results in a molecular complex of formic acid with 4 (4–FA). Despite a lower nucleophilicity of the HCOO^- moiety ($E_{\text{HOMO}(5^*)} = -6.10 \text{ eV}$, Fig. 5) compared to the C1 site in 2 ($E_{\text{HOMO}(2)} = -4.55 \text{ eV}$, Fig. 3), the direct availability of a proton-accepting species in the immediate vicinity of the dissociating H_2 molecule leads to a less strained TS_{5-4} transition state structure and, accordingly, to an extremely low activation barrier for the reaction. Indeed, the reactive moiety Ru–H–H in TS_{5-4} is characterized by substantially shorter interatomic distances ($r(\text{Ru}\cdots\text{H}) = 1.785 \text{ \AA}$ and $r(\text{H}\cdots\text{H}) = 0.920 \text{ \AA}$, Fig. 3) compared to the respective parameters in TS_{2-4} ($r(\text{Ru}\cdots\text{H}) = 1.881 \text{ \AA}$ and $r(\text{H}\cdots\text{H}) = 0.989 \text{ \AA}$, Fig. 3). Reaction of 4–FA with the DBU base at the next step releases DBU–FA product and regenerates the initial complex 4.

Alternatively, 5^* can rearrange to a stable complex 5 (ref. 67) ($5^* \rightarrow 5$, $\Delta E_{\text{ZPE}} = -39 \text{ kJ mol}^{-1}$, Fig. 3) featuring a direct Ru–O coordination ($r(\text{Ru–O}) = 2.261 \text{ \AA}$). Previously, this species has been proposed to be a resting state in the catalytic cycle by 4.⁴⁷ To proceed with the catalytic cycle (path I^a), the ionization of 5 (*i.e.* the formation of an ion pair 5^*) and the replacement of HCOO^- with H_2 has to take place. This reaction shows an activation barrier of 65 kJ mol^{-1} .



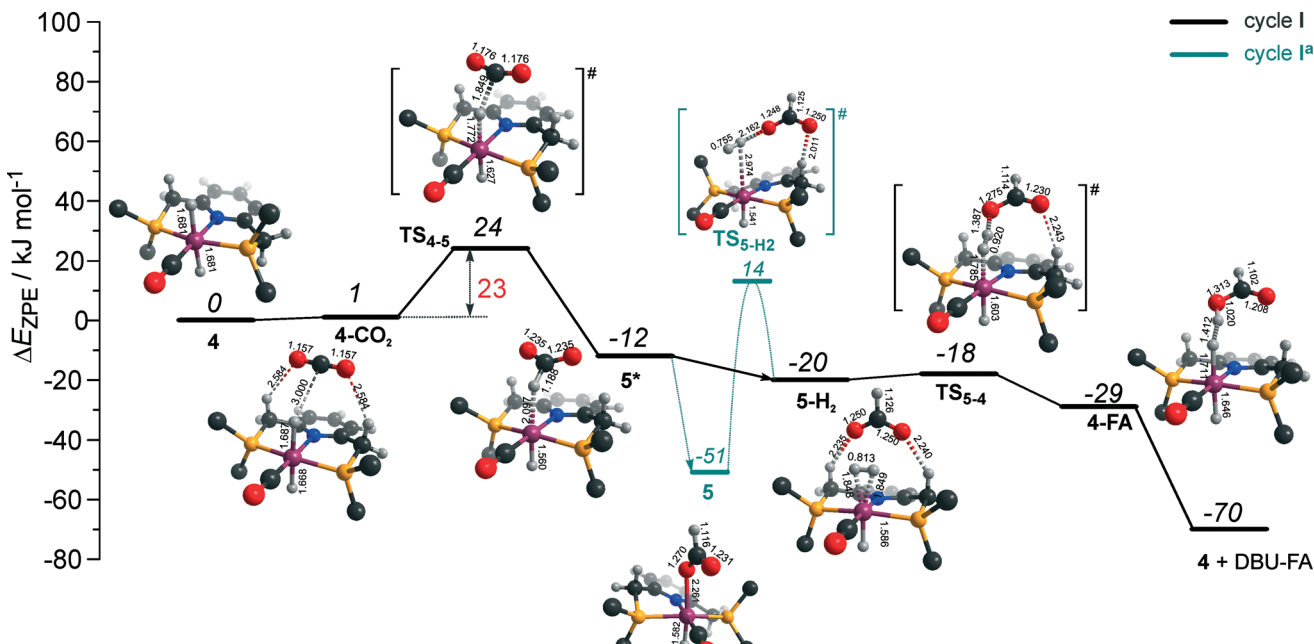


Fig. 3 DFT computed reaction energy diagram and optimized structures of the intermediate and transition states (CH_3 groups at the ^tBu substituents of the PNP ligand are omitted for clarity) for the hydrogenation of CO_2 over 4.⁴⁷

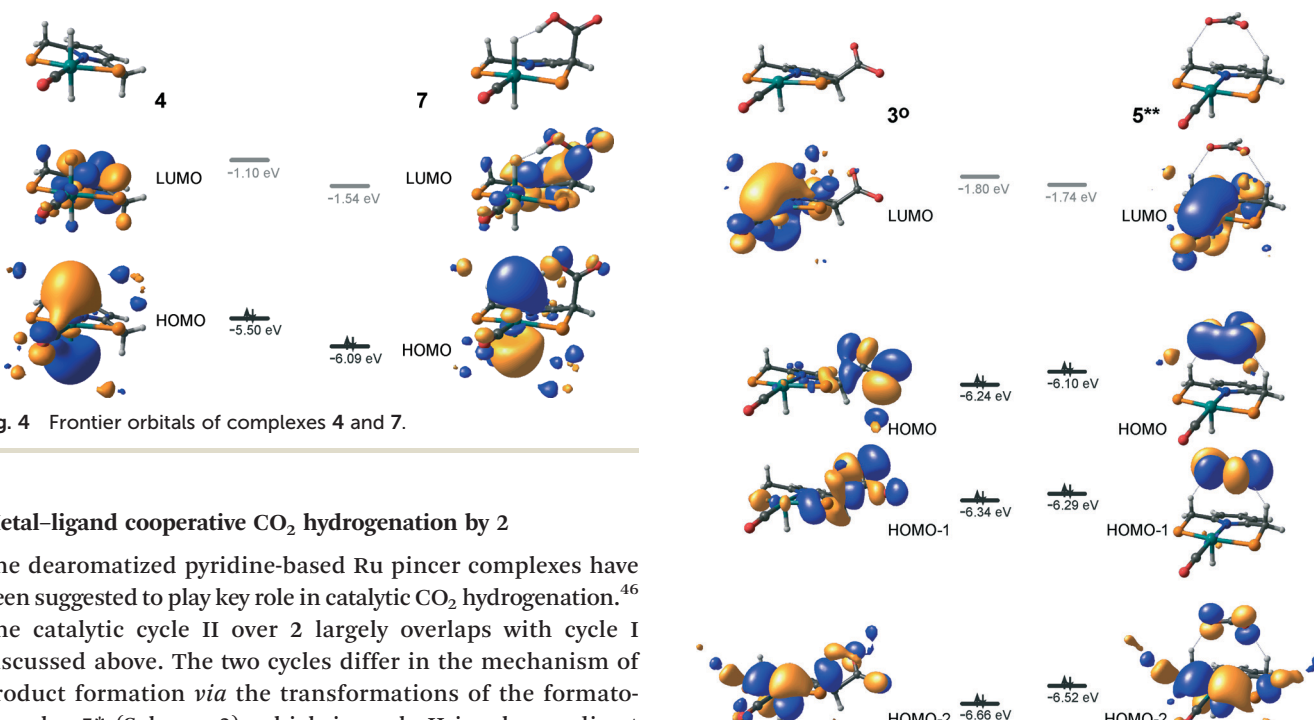


Fig. 4 Frontier orbitals of complexes 4 and 7.

Metal-ligand cooperative CO_2 hydrogenation by 2

The dearomatized pyridine-based Ru pincer complexes have been suggested to play key role in catalytic CO_2 hydrogenation.⁴⁶ The catalytic cycle II over 2 largely overlaps with cycle I discussed above. The two cycles differ in the mechanism of product formation *via* the transformations of the formato-complex 5^* (Scheme 2), which in cycle II involves a direct deprotonation of the PNP ligand resulting in a one-step FA formation. The DFT computed reaction energy diagram for CO_2 hydrogenation over 2 is shown in Fig. 6. Heterolytic dissociation of H_2 over 2 yielding 4 is the first and the most energy demanding step of the cycle ($E^\ddagger = 76 \text{ kJ mol}^{-1}$). It is followed by a facile CO_2 activation by the bis-hydrido species 4 resulting in 5^* . The weakly bound HCOO^- in 5^* plays then a role of a base that attacks the acidic CH_2 moiety at the PNP pincer arm resulting in its deprotonation and the

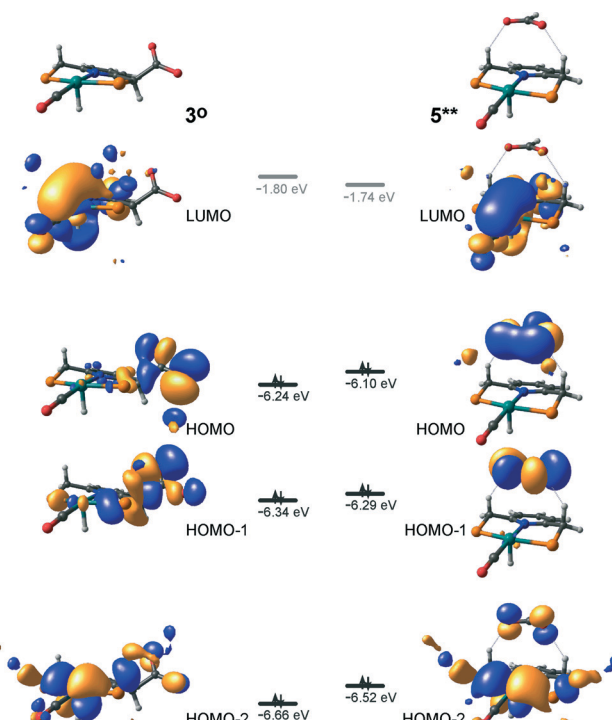


Fig. 5 Frontier orbitals of complexes 3° and 5**.

formation of FA molecule hydrogen-bonded with a basic C1 site at Ru-PNP* (2-FA). The reaction and activation energies are very similar for this step ($\Delta E_{\text{ZPE}} = 46 \text{ kJ mol}^{-1}$ and $E^\ddagger = 47 \text{ kJ mol}^{-1}$). Because of the very high basicity of the deprotonated pincer arm in 2, the reverse FA dissociation reaction is effectively barrierless. Therefore, to promote the

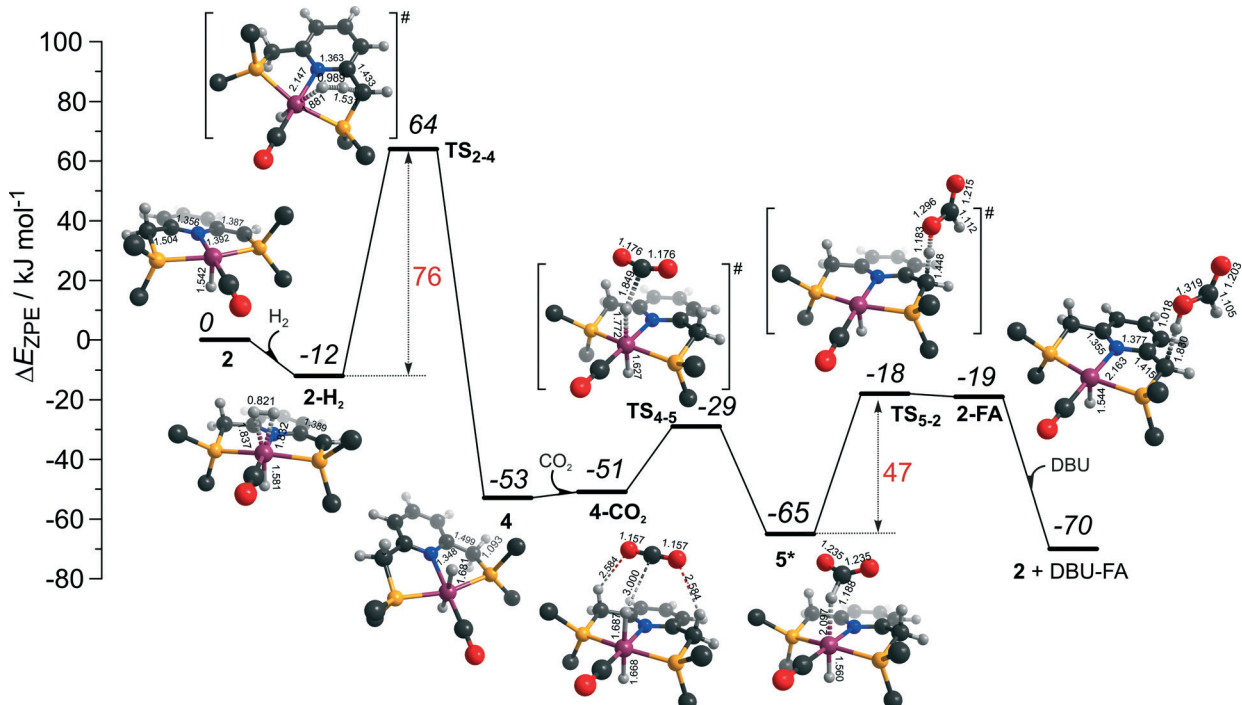


Fig. 6 DFT computed reaction energy diagram and optimized structures of the intermediate and transition states (CH₃ groups at the 'Bu substituents of the PNP ligand are omitted for clarity) for the direct hydrogenation of CO₂ over **2** (cycle II).⁴⁷

catalytic cycle FA has to be eliminated from the complex by a strongly exothermic ($\Delta E_{ZPE} = -51 \text{ kJ mol}^{-1}$) reaction with DBU base. The DBU-FA product is formed at this step and the original catalytic species 2 is regenerated.

CO₂ hydrogenation by 3

Potentially, the CO₂ adduct 3 can also act as catalytic species for CO₂ hydrogenation. In a very recent study by Huff and Sanford on the mechanism of CO₂ hydrogenation by a related Ru-PNN catalyst, the role of an Ru-PNN CO₂ adduct analogous to 3 has been discussed.⁴⁶ Although the mechanism for the catalytic reaction over such species was proposed, the authors concluded that it most likely represents a minor pathway in the overall catalytic process. The catalytic activity of the CO₂ adduct at elevated temperatures predominantly stems from the reversible binding of CO₂ that allows its transformations to a more reactive dearomatized Ru-PNN* complex under the catalytic conditions. Similarly, in the presence of H₂ or H₂-CO₂ mixture, 3 transforms directly to 5, from which cycle I^a can in principle be initiated. The catalytic activities of these complexes are very different⁴⁷ suggesting the principle possibility of the 3-catalyzed hydrogenation of CO₂.

The DFT-computed reaction energy diagram for the 3-catalyzed hydrogenation of CO_2 is shown in Fig. 7. To initiate the cycle III, complex 3 has to be activated *via* a rather unfavourable reaction ($\Delta E = 33 \text{ kJ mol}^{-1}$, $E^\ddagger = 69 \text{ kJ mol}^{-1}$) with H_2 that results in an opening of the Ru–O coordination and the formation of a 3°-H_2 . The coordinated dihydrogen molecule undergoes then a heterolytic dissociation over a cationic Ru center and the basic

carboxylate moiety on the pincer arm in 3°. The reaction in this case is less energetically favorable and proceeds with a higher barrier ($3^\circ\text{-H}_2 \rightarrow \text{TS}_{3-7} \rightarrow 7$, $\Delta E = 9 \text{ kJ mol}^{-1}$, $E^\ddagger = 15 \text{ kJ mol}^{-1}$) than the respective step in cycle I ($5\text{-H}_2 \rightarrow \text{TS}_{5-4} \rightarrow 4\text{-FA}$, $\Delta E = -9 \text{ kJ mol}^{-1}$, $E^\ddagger = 2 \text{ kJ mol}^{-1}$). This is in line with the differences in energies of the frontier orbitals (Fig. 5) and, accordingly, the acid-base properties, of the reactive moieties in these complexes. Reaction of 7 with CO_2 yields a formato-complex 8 that resembles 5* in cycle I. This step is slightly endothermic ($\Delta E = 4 \text{ kJ mol}^{-1}$) and shows an activation barrier of 45 kJ mol^{-1} . The lower reactivity of 7 towards CO_2 compared to that of catalyst 4 stems from the decreased hydricity of the Ru-H moiety interacting with the carboxylic acid group at the pincer arm of 7 (Fig. 4). Subsequent barrierless proton transfer from the ligand-bound $-\text{COOH}$ moiety to the HCOO^- anion in 8 results in FA hydrogen-bonded to the activated complex 3° (FA-3°). The removal of FA by the reaction with DBU regenerates the initial CO_2 -adduct 3.

Implications for catalysis

The computational results presented above suggest that all candidate Ru-PNP complexes 2–4 can be formed under the CO_2 hydrogenation conditions and may contribute to the overall catalytic reaction. To directly compare the above three alternative mechanism for CO_2 hydrogenation by Ru-PNP, we further analysed reaction Gibbs free energy diagrams for these three catalytic cycles (Fig. 8).

The bis-hydrido complex 4 provides the lowest free energy reaction path for the conversion of CO_2 to FA-DBU along the cycle I (Fig. 8). The reaction in this case does not involve the

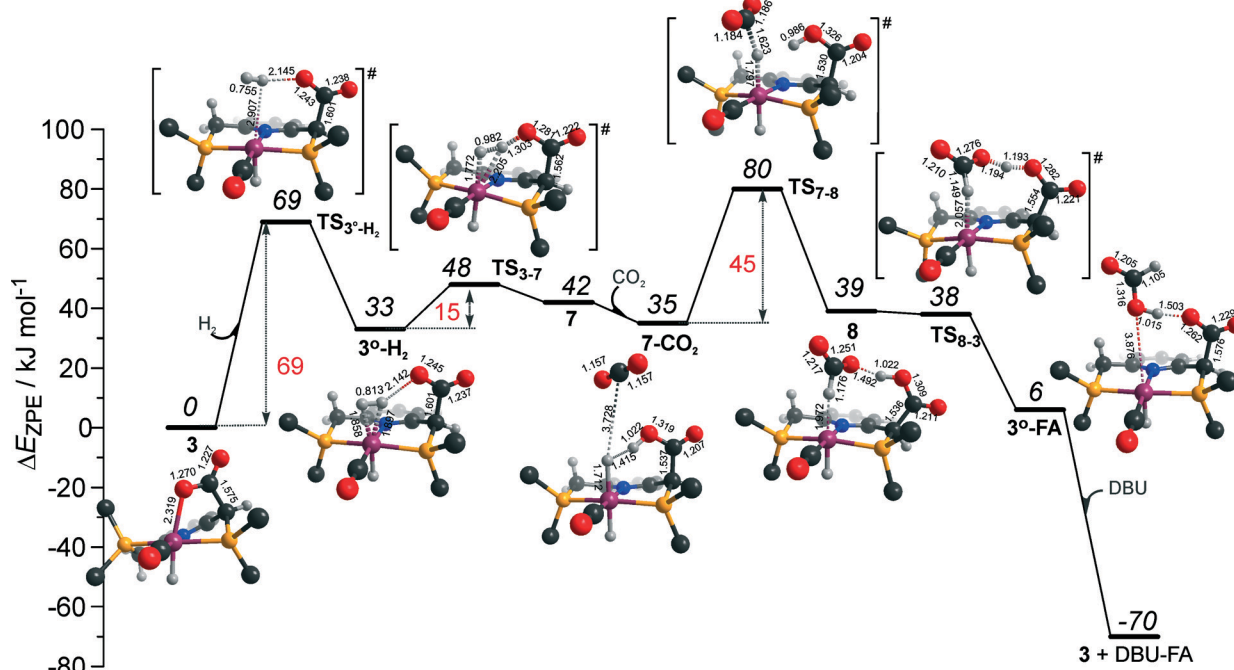


Fig. 7 DFT computed reaction energy diagram and optimized structures of the intermediate and transition states (CH_3 groups at the ^tBu substituents of the PNP ligand are omitted for clarity) for the direct hydrogenation of CO_2 over 3 (cycle III).

metal-ligand cooperation in Ru-PNP and proceeds *via* the direct hydrogenolysis of transient species 5^* containing a non-coordinated formate anion ($5^* + \text{H}_2 \rightarrow 5-\text{H}_2 \rightarrow 4-\text{FA}$, Fig. 3 and 8). DFT calculations predict that the reaction along

this path shows a very low apparent activation energy⁶⁸ of 24 kJ mol^{-1} ($4 + \text{CO}_2 \rightarrow 5^*$, Fig. 3) associated with the initial CO_2 activation step. The free energy barrier ΔG^\ddagger for this transformation is 67 kJ mol^{-1} (Fig. 8). The subsequent facile

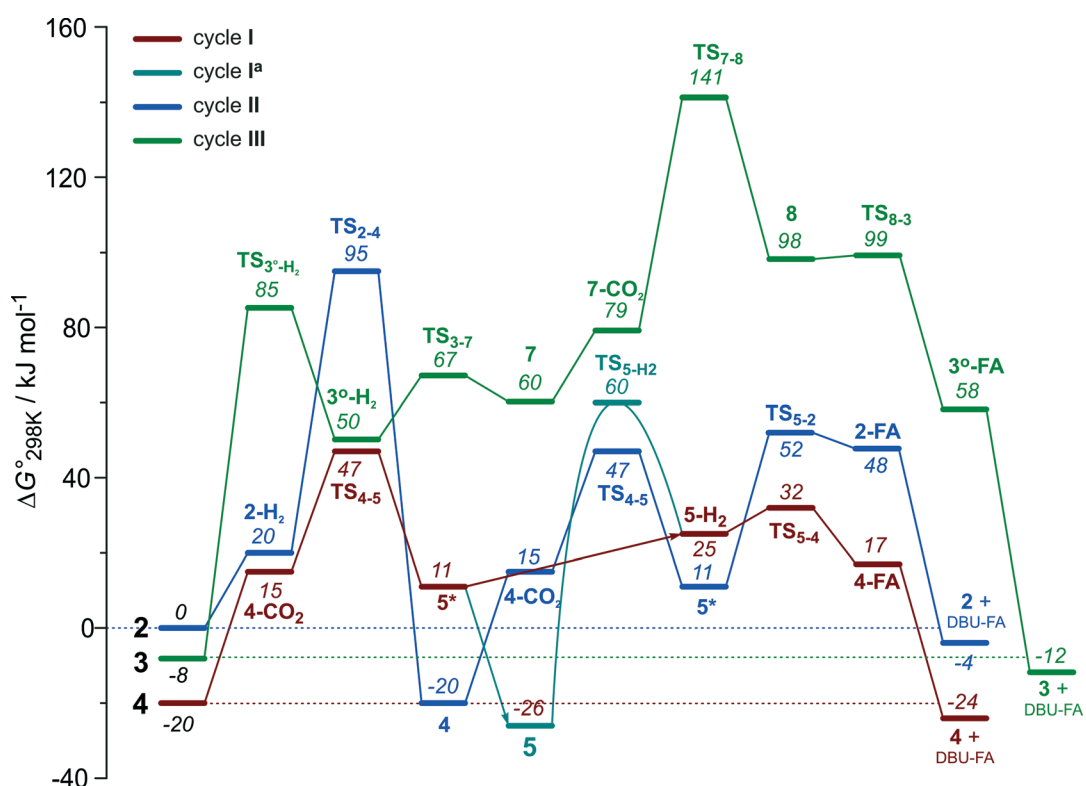


Fig. 8 A comparison of Gibbs free energy diagrams for catalytic cycles I, II and III plotted relative to the dearomatized Ru-PNP* species 2.



hydrogenolysis of 5^* is competing with its rearrangement to a formato-complex 5 . 5 is the most thermodynamically stable species among the Ru-PNP intermediates considered here. This finding is in line with the results of experimental ^1H NMR reactivity studies evidencing the exclusive formation of 5 under near-catalytic conditions.⁴⁷ The polarization of 5 followed by H_2 insertion ($5 + \text{H}_2 \rightarrow 5\text{-H}_2$, Fig. 3) is the rate-determining step (RDS) of the catalytic mechanism involving the formation of 5 (cycle I^a). This route is characterized by $E_{\text{app}}^{\ddagger, \text{DFT}}$ of 65 kJ mol^{-1} that is comparable to the activation energies predicted for the elementary reaction steps involved in the alternative catalytic cycles II and III promoted by, respectively, complexes 2 and 3 .

The data in Fig. 6 and 8 suggest that the cooperative H_2 activation by 2 represents the RDS of the MLC mechanism along the cycle II. Since the formation of an 2-H_2 σ -complex is thermodynamically unfavourable, this route should proceed with a moderate $E_{\text{app}}^{\ddagger, \text{DFT}}$ of 64 kJ mol^{-1} ($2 + \text{H}_2 \rightarrow 4$, Fig. 6). In free energy terms this pathway shows a rather high free energy barrier of 95 kJ mol^{-1} ($2 + \text{H}_2 \rightarrow 4$, Fig. 8). The catalysis on the CO_2 adduct 3 (cycle III) proceeds *via* a sequence of thermodynamically unfavourable steps (Fig. 8). Although the initial coordination of H_2 ($3 + \text{H}_2 \rightarrow 3^\circ\text{-H}_2$, Fig. 7) shows an activation energy (E^\ddagger) of only 69 kJ mol^{-1} , the overall barrier in this case is represented by the energy difference between the initial state 3 and the high energy TS_{7-8} for the CO_2 activation ($E_{\text{app}}^{\ddagger, \text{DFT}} = 80 \text{ kJ mol}^{-1}$ Fig. 7, $\Delta G_{\text{app}}^{\ddagger, \text{DFT}} = 149 \text{ kJ mol}^{-1}$ Fig. 8). In line with the experimental findings,⁴⁷ this points to a lower catalytic activity of 3 compared to that of 2 and 4 . Under the catalytic conditions, the contribution of 2 is limited due to the low thermodynamic stability of the reaction intermediates and high activation free energy barriers along the respective MLC path II.

Catalytic CO_2 hydrogenation experiments with Ru-PNP catalyst precursor 1 and a strong $\text{KO}^\ddagger\text{Bu}$ support this proposition. We propose that $\text{KO}^\ddagger\text{Bu}$ can promote the dearomatization of the PNP pincer ligand⁶⁰ in the stable intermediates formed in the course of the reaction towards Ru-PNP* complex 2 and therefore ensure the high steady-state concentration of this activated complex under the catalytic conditions. Independent of the reaction medium, a very low activity was observed in this case. Turnover numbers after 2 hour reaction (TON(2 h)) were only 728 and 649 in THF and DMF solvents, respectively. On contrary, when a non-nucleophilic DBU base, which cannot promote the ligand dearomatization,⁴⁷ was used as a promoter, much higher TON(2 h) values of $12\,829$ and $38\,642$ in THF and DMF solvents, respectively, were obtained (Table S1, ESI[†]).

The catalytic CO_2 hydrogenation by Ru-PNP complexes is dominated by the competing reaction paths I and I^a realized by the bis-hydrido Ru-PNP complex 4 . These paths are differentiated by the mechanism of the transformation of the polarized formate complex 5^* . The competing rearrangement ($5^* \rightarrow 5$, path I^a) and hydrogenolysis ($5^* + \text{H}_2 + \text{DBU} \rightarrow 4 + \text{FA-DBU}$, path I) routes show similar reaction free energy changes (Fig. 8) and involve effectively barrierless transformations (Fig. 3). We therefore speculate that the latter mechanism can

be promoted in the presence of an excess H_2 that would ensure the rapid substitution of the non-coordinated HCOO^- and its replacement with H_2 towards 5-H_2 .

To verify this hypothesis, we investigated the kinetics of CO_2 hydrogenation by Ru-PNP complex 1 (Fig. 9) in the presence of DBU with varying H_2/CO_2 molar ratio ($p_{\text{total}} = 40 \text{ bar}$). At a H_2/CO_2 molar ratio of $3/1$, the reaction showed an apparent activation energy ($E_{\text{app}}^{\ddagger}$) of 57 kJ mol^{-1} that is in very good agreement with the computed value ($E_{\text{app}}^{\ddagger, \text{DFT}}$) of 65 kJ mol^{-1} for cycle I^a (Fig. 3).

The rate enhancement previously observed upon a slight increase of the partial pressure of H_2 (ref. 22) is in line with the proposition on the rate-determining nature of the $5 + \text{H}_2 \rightarrow 5\text{-H}_2$ step in this case. As a result of the high activation energy, a strong temperature dependency of the reaction rate is observed. Whereas the reaction at 132°C shows an initial turnover frequency (TOF) of $1\,892\,000 \text{ h}^{-1}$, the initial TOF at 90°C is only $266\,000 \text{ h}^{-1}$. When the reaction is carried out in the presence of a large excess of H_2 ($\text{H}_2/\text{CO}_2 = 37/3$), the apparent activation energy drops to only 20 kJ mol^{-1} , which is in perfect agreement with the value of 24 mol^{-1} predicted for the direct hydrogenolysis path I (Fig. 3). At a temperature of 129°C , the reaction shows a TOF of $1\,099\,000 \text{ h}^{-1}$. In line with the proposal on the RDS nature of the CO_2 activation step in cycle I, the lower reaction rate for a high temperature

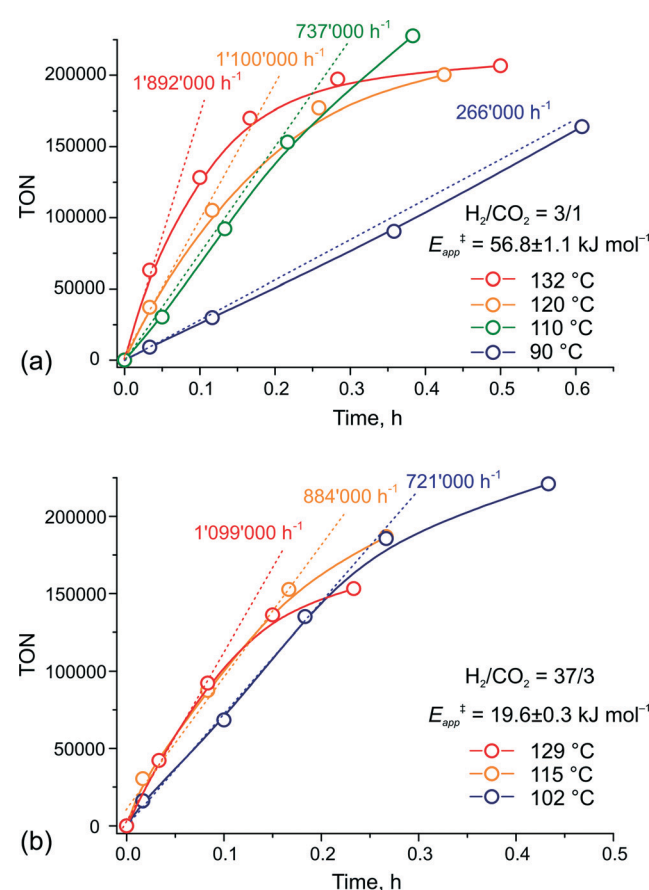


Fig. 9 Kinetic traces for CO_2 hydrogenation by 1 at different temperatures and H_2/CO_2 ratio of (a) $3/1$ and (b) $37/3$ ($p_{\text{total}} = 40 \text{ bar}$).



reaction in this case is most likely due to the decreased partial pressure of CO_2 . An important consequence of the low activation barrier for CO_2 hydrogenation at a high H_2/CO_2 molar ratio is the possibility to achieve high rates of the catalytic reaction at lower temperatures (Fig. 9(b)). An initial rate of 721 000 h^{-1} was obtained at 102 °C. From the Arrhenius plot one can estimate TOF values above 100 000 h^{-1} to be reachable at ambient temperature. These findings render the Ru-PNP complex **1** in combination with non-nucleophilic DBU base one of the most active CO_2 hydrogenation catalytic system reported to date.

Conclusions

The mechanism of CO_2 hydrogenation to DBU formate salt in the presence of homogeneous pyridine-based Ru-PNP pincer catalysts was investigated by means of density functional theory calculations. The focus was on unravelling the complexity of the underlying reaction mechanisms and determining the routes for the optimization of the performance of this catalytic system. Dedicated catalytic tests and kinetic study were carried out to verify the theoretical predictions.

Three major interconnected reaction paths catalysed by dearomatised Ru-PNP* complex **2** or by its cooperative adducts with CO_2 and H_2 , Ru-PNP complexes **3** and **4**, respectively, were considered. On the basis of the theoretical results it is proposed that depending on the reaction conditions, the relative concentration of these reactive species and their contribution to the overall catalytic performance varies. Whereas formation of **4** upon the reaction of **2** with H_2 is thermodynamically preferred, the competing [1,3]- CO_2 addition towards **3** is favoured kinetically. We propose that the latter route will dominate in excess strong base needed to ensure a high steady-state concentration of the activated precursor **2** and a high partial pressure of CO_2 . At increased H_2 partial pressure, the reaction will be driven towards the most stable dihydrido-Ru-PNP complex.

The hydrogenation of CO_2 catalysed by **3** proceeds *via* a sequence of highly endothermic elementary steps showing also rather high activation barriers. As a result, the highest apparent activation barrier of 80 kJ mol^{-1} is predicted for the respective catalytic cycle III. This cycle is also characterized by a prohibitively high overall Gibbs free energy barrier of 149 kJ mol^{-1} . In the case of the catalysis by the dearomatised species **2**, metal-ligand cooperation plays an important role in the reaction mechanism. The initial heterolytic H_2 dissociation over an acid-base pair formed by the 5-coordinated Ru centre and the deprotonated CH basic site at the PNP* pincer arm is the rate-determining step ($E_{\text{app}}^{\ddagger, \text{DFT}} = 64 \text{ kJ mol}^{-1}$, $\Delta G_{\text{app}}^{\ddagger, \text{DFT}} = 95 \text{ kJ mol}^{-1}$). Despite the high intrinsic reactivity of the acid and base sites in Ru-PNP*, their distant location within the rigid dearomatised pincer complex strongly hamper the heterolytic H_2 dissociation. When a much less basic HCOO^- anion acts as the basic site in related steps over **3*** (cycle III) and **5*** (cycle I) complexes, much lower activation barriers are predicted. Most of the reaction intermediates involved in the catalytic cycles II and III are rather unstable

thermodynamically and their transformations proceed with rather high free energy barriers. This suggests only minor contribution of these reaction paths under common CO_2 hydrogenation conditions.

DFT calculations predict that the bis-hydrido Ru-PNP complex **4** is the most active one. CO_2 hydrogenation by **4** can follow two mechanisms (cycle I and I^a) that do not involve metal-ligand cooperative steps. A facile CO_2 activation by Ru-H moiety resulting in a non-coordinated HCOO^- and a 5-coordinated cationic Ru-PNP (**5*** represents the initial step in both catalytic cycle. The cycles are distinguished by the mechanism of the subsequent transformations of **5*** that, in turn, depends on the partial pressure of H_2 . Under excess H_2 , the substitution of the non-coordinated HCOO^- anion in **5*** with H_2 resulting in a σ -complex **5**- H_2 initiates an almost barrierless sequence of elementary steps towards the completion of the catalytic cycle and the formation of the FA-DBU product. The competing route I^a involves the rearrangement of **5*** towards a stable formato-complex **5** that has previously been proposed to be the resting state of the catalytic reaction. The polarization of **5** followed by H_2 insertion to yield **5*** determines the overall reaction rate for the I^a mechanism and shows an activation barrier of 65 kJ mol^{-1} . The initial CO_2 activation is the rate-determining step in cycle I, for which an apparent activation energy of only 24 kJ mol^{-1} is predicted.

The analysis of experimental reaction kinetics for CO_2 hydrogenation by Ru-PNP confirms these theoretical predictions. By increasing the molar H_2/CO_2 ratio in the catalytic experiment from 3/1 to 37/3, the apparent activation energy decreases from 57 to 20 kJ mol^{-1} , respectively, in a perfect agreement with the computed values. A relatively small temperature dependency of the reaction rate in the latter case points to the possibility of achieving very high catalytic performance in CO_2 hydrogenation by Ru-PNP under near-ambient temperatures.

Acknowledgements

E.A.P. gratefully acknowledges the Technology Foundation STW and the Netherlands Organization for Scientific Research (NWO) for his personal VENI grant. SurfSARA and NWO are acknowledged for providing access to supercomputer resources (grant SH-231). The authors thank Dr. L. Leffort (DSM) for the possibility to carry out high-throughput experiments.

Notes and references

- 1 M. Cokoja, C. Bruckmeier, B. Rieger, W. A. Herrmann and F. E. Kühn, *Angew. Chem., Int. Ed.*, 2011, **50**, 8510–8537.
- 2 K. Huang, C.-L. Sun and Z.-J. Shi, *Chem. Soc. Rev.*, 2011, **40**, 2435–2452.
- 3 T. Sakakura, J.-C. Choi and H. Yasuda, *Chem. Rev.*, 2007, **107**, 2365–2387.
- 4 C. Maeda, Y. Miyazaki and T. Ema, *Catal. Sci. Technol.*, 2014, **4**, 1482–1497.

5 C. J. Whiteoak, N. Kielland, V. Laserna, E. C. Escudero-Adán, E. Martin and A. W. Kleij, *J. Am. Chem. Soc.*, 2013, **135**, 1228–1231.

6 M. L. Lejkowski, R. Lindner, T. Kageyama, G. É. Bódizs, P. N. Plessow, I. B. Müller, A. Schäfer, F. Rominger, P. Hofmann, C. Futter, S. A. Schunk and M. Limbach, *Chem. – Eur. J.*, 2012, **18**, 14017–14025.

7 L. Zhang, J. Cheng, B. Carry and Z. Hou, *J. Am. Chem. Soc.*, 2012, **134**, 14314–14317.

8 B. Chatelet, L. Joucla, J.-P. Dutasta, A. Martinez, K. C. Szeto and V. Dufaud, *J. Am. Chem. Soc.*, 2013, **135**, 5348–5351.

9 T. Sakai, Y. Tsutsumi and T. Ema, *Green Chem.*, 2008, **10**, 337–341.

10 L. Wu, Q. Liu, I. Fleischer, R. Jackstell and M. Beller, *Nat. Commun.*, 2014, **5**, 3091.

11 C. Federsel, R. Jackstell and M. Beller, *Angew. Chem., Int. Ed.*, 2010, **49**, 6254–6257.

12 J. F. Hull, Y. Himeda, W.-H. Wang, B. Hashiguchi, R. Periana, D. J. Szalda, J. T. Muckerman and E. Fujita, *Nat. Chem.*, 2012, **4**, 383–388.

13 C. A. Huff and M. S. Sanford, *J. Am. Chem. Soc.*, 2011, **133**, 18122–18125.

14 S. Wesselbaum, T. vom Stein, J. Klankermayer and W. Leitner, *Angew. Chem., Int. Ed.*, 2012, **51**, 7499–7502.

15 Y.-N. Li, R. Ma, L.-N. He and Z.-F. Diao, *Catal. Sci. Technol.*, 2014, **4**, 1498–1512.

16 M. Nielsen, E. Alberico, W. Baumann, H.-J. Drexler, H. Junge, S. Gladiali and M. Beller, *Nature*, 2013, **495**, 85–89.

17 R. E. Rodríguez-Lugo, M. Trincado, M. Vogt, F. Tewes, G. Santiso-Quinones and H. Grützmacher, *Nat. Chem.*, 2013, **5**, 342–347.

18 F. Joó, *ChemSusChem*, 2008, **1**, 805–808.

19 S. Enthaler, *ChemSusChem*, 2008, **1**, 801–804.

20 A. Boddien, F. Gaertner, C. Federsel, P. Sponholz, D. Mellmann, R. Jackstell, H. Junge and M. Beller, *Angew. Chem., Int. Ed.*, 2011, **50**, 6411–6414.

21 C. Fellay, P. J. Dyson and G. Laurenczy, *Angew. Chem., Int. Ed.*, 2008, **47**, 3966–3968.

22 G. A. Filonenko, R. van Putten, E. N. Schulpen, E. J. M. Hensen and E. A. Pidko, *ChemCatChem*, 2014, **6**, 1526–1530.

23 A. Boddien, C. Federsel, P. Sponholz, D. Mellmann, R. Jackstell, H. Junge, G. Laurenczy and M. Beller, *Energy Environ. Sci.*, 2012, **5**, 8907–8911.

24 S.-F. Hsu, S. Rommel, P. Eversfield, K. Muller, E. Klemm, W. R. Thiel and B. Plietker, *Angew. Chem., Int. Ed.*, 2014, DOI: 10.1002/anie.201310972.

25 M. Drees, M. Cokoja and F. E. Kühn, *ChemCatChem*, 2012, **4**, 1703–1712.

26 T. Fan, X. Chen and Z. Lin, *Chem. Commun.*, 2012, **48**, 10808–10828.

27 C. Creutz, M. H. Chou, H. Hou and J. T. Muckerman, *Inorg. Chem.*, 2010, **49**, 9809–9822.

28 K.-W. Huang, J. H. Han, C. B. Musgrave and E. Fujita, *Organometallics*, 2006, **26**, 508–513.

29 T. Schaub and R. A. Paciello, *Angew. Chem., Int. Ed.*, 2011, **50**, 7278–7282.

30 C. Federsel, R. Jackstell and M. Beller, *Angew. Chem., Int. Ed.*, 2010, **49**, 6254–6257.

31 W. Wang, S. Wang, X. Ma and J. Gong, *Chem. Soc. Rev.*, 2011, **40**, 3703–3727.

32 R. Langer, Y. Diskin-Posner, G. Leitus, L. J. W. Shimon, Y. Ben-David and D. Milstein, *Angew. Chem., Int. Ed.*, 2011, **50**, 9948–9952.

33 C. Ziebart, C. Federsel, P. Anbarasan, R. Jackstell, W. Baumann, A. Spannenberg and M. Beller, *J. Am. Chem. Soc.*, 2012, **134**, 20701–20704.

34 M. S. Jeletic, M. T. Mock, A. M. Appel and J. C. Linehan, *J. Am. Chem. Soc.*, 2013, **135**, 11533–11536.

35 P. Munshi, A. D. Main, J. C. Linehan, C.-C. Tai and P. G. Jessop, *J. Am. Chem. Soc.*, 2002, **124**, 7963–7971.

36 Y.-Y. Ohnishi, T. Matsunaga, Y. Nakao, H. Sato and S. Sakaki, *J. Am. Chem. Soc.*, 2005, **127**, 4021–4032.

37 Y.-Y. Ohnishi, Y. Nakao, H. Sato and S. Sakaki, *Organometallics*, 2006, **25**, 3352–3363.

38 A. Urakawa, F. Jutz, G. Laurenczy and A. Baiker, *Chem. – Eur. J.*, 2007, **13**, 3886–3899.

39 R. Tanaka, M. Yamashita and K. Nozaki, *J. Am. Chem. Soc.*, 2009, **131**, 14168–14169.

40 C. Gunanathan and D. Milstein, *Acc. Chem. Res.*, 2011, **44**, 588–602.

41 J. I. van der Vlugt and J. N. H. Reek, *Angew. Chem., Int. Ed.*, 2009, **48**, 8832–8846.

42 E. Balaraman and D. Milstein, *Top. Organomet. Chem.*, 2014, **77**, 1–25.

43 R. Tanaka, M. Yamashita, L. W. Chung, K. Morokuma and K. Nozaki, *Organometallics*, 2011, **30**, 6742–6750.

44 X. Yang, *ACS Catal.*, 2011, **1**, 849–854.

45 M. S. G. Ahlquist, *J. Mol. Catal. A: Chem.*, 2010, **324**, 3–8.

46 C. A. Huff and M. S. Sanford, *ACS Catal.*, 2013, **3**, 2412–2416.

47 G. A. Filonenko, M. P. Conley, C. Copéret, M. Lutz, E. J. M. Hensen and E. A. Pidko, *ACS Catal.*, 2013, **3**, 2522–2526.

48 C. A. Huff, J. W. Kampf and M. S. Sanford, *Organometallics*, 2012, **31**, 4643–4645.

49 M. Vogt, M. Gargir, M. A. Iron, Y. Diskin-Posner, Y. Ben-David and D. Milstein, *Chem. – Eur. J.*, 2012, **18**, 9194–9197.

50 J. Zhang, G. Leitus, Y. Ben-David and D. Milstein, *Angew. Chem., Int. Ed.*, 2006, **45**, 1113–1115.

51 C. Adamo and V. Barone, *J. Chem. Phys.*, 1999, **110**, 6158–6170.

52 *Gaussian 09 Revision D.01*, M. J. Frisch, G. W. Trucks, H. B. Schlegel, G. E. Scuseria, M. A. Robb, J. R. Cheeseman, G. Scalmani, V. Barone, B. Mennucci, G. A. Petersson, H. Nakatsuji, M. Caricato, X. Li, H. P. Hratchian, A. F. Izmaylov, J. Bloino, G. Zheng, J. L. Sonnenberg, M. Hada, M. Ehara, K. Toyota, R. Fukuda, J. Hasegawa, M. Ishida, T. Nakajima, Y. Honda, O. Kitao, H. Nakai, T. Vreven, J. A. Montgomery Jr., J. E. Peralta, F. Ogliaro, M. Bearpark, J. J. Heyd, E. Brothers, K. N. Kudin,



V. N. Staroverov, R. Kobayashi, J. Normand, K. Raghavachari, A. Rendell, J. C. Burant, S. S. Iyengar, J. Tomasi, M. Cossi, N. Rega, N. J. Millam, M. Klene, J. E. Knox, J. B. Cross, V. Bakken, C. Adamo, J. Jaramillo, R. Gomperts, R. E. Stratmann, O. Yazev, A. J. Austin, R. Cammi, C. Pomelli, J. W. Ochterski, R. L. Martin, K. Morokuma, V. G. Zakrzewski, G. A. Voth, P. Salvador, J. J. Dannenberg, S. Dapprich, A. D. Daniels, Ö. Farkas, J. B. Foresman, J. V. Ortiz, J. Cioslowski and D. J. Fox, Gaussian, Inc., Wallingford CT, 2009.

53 Y. Zhao and D. G. Truhlar, *J. Chem. Theory Comput.*, 2009, **5**, 324–333.

54 R. Valero, R. Costa, I. de P. R. Moreira, D. G. Truhlar and F. Illas, *J. Chem. Phys.*, 2008, **128**, 114003.

55 R. Krishnan, J. S. Binkley, R. Seeger and J. A. Pople, *J. Chem. Phys.*, 1980, **72**, 650–654.

56 A. D. McLean and G. S. Chandler, *J. Chem. Phys.*, 1980, **72**, 5639–5648.

57 P. J. Hay and W. R. Wadt, *J. Chem. Phys.*, 1985, **82**, 270–283.

58 P. J. Hay and W. R. Wadt, *J. Chem. Phys.*, 1985, **82**, 299–310.

59 D. Andrae, U. Häußermann, M. Dolg, H. Stoll and H. Preuß, *Theor. Chim. Acta*, 1990, **77**, 123–141.

60 B. Gnanaprakasam, J. Zhang and D. Milstein, *Angew. Chem., Int. Ed.*, 2010, **49**, 1468–1471.

61 E. Khaskin, M. A. Iron, L. J. W. Shimon, J. Zhang and D. Milstein, *J. Am. Chem. Soc.*, 2010, **132**, 8542–8543.

62 J. Kubas Gregory, *Acc. Chem. Res.*, 1988, **21**, 120–128.

63 V. B. Kazansky and E. A. Pidko, *Catal. Today*, 2005, **110**, 281–293.

64 R. H. Crabtree and M. Lavin, *J. Chem. Soc., Chem. Commun.*, 1985, 1661–1662.

65 R. H. Crabtree, *Acc. Chem. Res.*, 1990, **23**, 95–101.

66 G. Alcaraz, M. Grellier and S. Sabo-Etienne, *Acc. Chem. Res.*, 2009, **42**, 1640–1649.

67 M. Ahlquist, G. Fabrizi, S. Cacchi and P.-O. Norrby, *J. Am. Chem. Soc.*, 2006, **128**, 12785–12793.

68 $E_{\text{app}}^{\ddagger, \text{DFT}}$ is defined as the difference in ZPE-corrected energy of the species corresponding to the highest and the lowest energy point in the reaction Gibbs free energy diagram for a particular proposed catalytic cycle (Fig. 8).

